

Understanding the Unusually Straight: A Search For MO Insights into Linear {FeNO}⁷ Units

Jeanet Conradie,^{†,‡} Kathrin H. Hopmann,[†] and Abhik Ghosh*,[†]

Department of Chemistry and Center for Theoretical and Computational Chemistry, University of Tromsø, N-9037 Tromsø, Norway, and Department of Chemistry, University of the Free State, 9300 Bloemfontein, Republic of South Africa

Received: March 1, 2010; Revised Manuscript Received: May 6, 2010

Ferrous-nitrosyl {FeNO}⁷ complexes, whether $S = 1/2$ or $3/2$, generally exhibit bent FeNO angles of around $140\text{--}145^\circ$. There are, however, a handful of exceptions, which are characterized by linear or quasi-linear FeNO units. Presented herein is a relatively comprehensive DFT-based MO analysis of these unusual {FeNO}⁷ complexes. DFT-derived FeNO bending potentials indicate that the unusual, experimentally observed quasi-linear geometries indeed correspond to minimum-energy structures on the potential energy surfaces of the isolated molecules/ions. Walsh diagram analyses support our earlier suggestion that the linearity of the {FeNO}⁷ units in question is most commonly attributable metal d_σ - p_σ mixing resulting from the lack of a ligand trans to the NO. Importantly, this effect explains the linearity of both $S = 1/2$ {FeNO}⁷ complexes such as [Fe(CN)₄(NO)]²⁻ and Fe(dtc-Me₂)₂(NO) (dtc-Me₂ = *N,N'*-dimethylidithiocarbamate) and $S = 3/2$ complexes such as [Fe(S'Bu)₃(NO)]⁻. However, Roussin's black salt anion, [Fe₄(μ -S)₃(NO)₇]⁻, which also contains a linear {FeNO}⁷ unit, entails additional, special metal-ligand orbital interactions. The well-known brown-ring complex [Fe(H₂O)₅(NO)]²⁺ also contains a linear {FeNO}⁷ unit; the linearity in this case is attributable to the weakness of the trans water ligand.

Introduction

Nitrosylhemes, the paradigms of {FeNO}⁷ complexes,¹ are invariably $S = 1/2$ species with FeNO angles of about 140° .^{2–5} The significantly bent angle is most simply viewed as resulting from a σ interaction between the Fe d_{z^2} orbital and an NO π^* orbital.^{6–8} The same orbital interaction is also present in a number of $S = 3/2$, trigonal-bipyramidal nonheme {FeNO}⁷ complexes with bent, axial NO groups.⁹ Against this broad context, a handful of nonheme {FeNO}⁷ complexes, both $S = 1/2$ and $3/2$, stand out, which are characterized by essentially linear {FeNO}⁷ groups. Thus, the two $S = 1/2$ complexes [Fe(CN)₄(NO)]²⁻ and Fe(dtc-Me₂)₂(NO) (dtc-Me₂ = *N,N'*-dimethylidithiocarbamate) feature strictly linear FeNO units.^{10,11} Key examples of structurally characterized, $S = 3/2$ species with linear FeNO groups include anionic, pseudotetrahedral tris(thiolato)^{12,13} and triscarboxylato-{FeNO}⁷ complexes.¹⁴ To this list must be added the well-known $S = 0$ Roussin's black salt anion, [Fe₄(μ -S)₃(NO)₇]⁻,^{15–19} whose unique linear FeNO unit is believed to be (locally) an $S = 3/2$, {FeNO}⁷ center. Now, although some of these systems have been studied by quantum chemical methods,^{9,11,18} no comprehensive theoretical study has been reported so far, which provided the key motivation for this study. Figure 1 depicts the various molecules (A–H) and ions that we have examined with DFT calculations in this study.

The above, structurally characterized complexes with linear {FeNO}⁷ groups appear to share another structural feature: they all lack axial ligands trans to the NO.^{9,11,18} Indeed, we suggested a causal relationship between the two structural features. In a number of cases, the lack of a trans ligand results in metal p_z

character mixing into the d_σ -based HOMO, which reduces the antibonding interaction between the metal and the NO lone pair, which in turn leads to a linear FeNO unit.^{9,11,18} Figure 2 depicts this metal d_σ -based HOMO for the various molecules studied. In this study, we have examined two major aspects of linear or quasi-linear {FeNO}⁷ groups. First, we wished to take a more critical look at the available crystallographic results or, more accurately, at the implications thereof. The handful of relevant structural studies do not indicate whether the observed quasi-linear geometries reflect the inherent conformational preference of the {FeNO}⁷ units in question, or whether they are somehow dictated by crystal packing forces.^{10,12–14} To address this issue, we have evaluated the FeNO bending potentials of all of the molecules examined using a consistent method (OLYP^{20,21}/STO-TZP). The results allow a comparison of the flexibility of $S = 1/2$ and $3/2$ {FeNO}⁷ units with regard to FeNO bending, a point on which little information is available in the literature.²² Second, we also wished to examine more critically the tentative MO arguments^{9,11,17,18} that we have put forward to explain the linearity of the {FeNO}⁷ units in question. We have done so here using a Walsh diagram approach, where the orbital energies of various metal d -based occupied MOs were tracked as a function of the FeNO angle. Gratifyingly, our original insight with regard to the HOMO topology as an indicator of {FeNO}⁷ stereochemistry emerges essentially unchanged from this analysis.²³

A couple of inorganic chemistry's iconic complexes were also examined as part of this study. Roussin's black salt anion is of particular interest as it raises the question whether its unique spin-coupled electronic structure has a significant effect on the FeNO bending potential. It appears that this is indeed the case, as described below. Second, DFT calculations predict a linear {FeNO}⁷ unit for the well-known brown ring complex, [Fe(H₂O)₅(NO)]²⁺, an octahedral complex with a water ligand

* To whom correspondence should be addressed. E-mail: abhik@chem.uit.no.

[†] University of Tromsø.

[‡] University of the Free State.

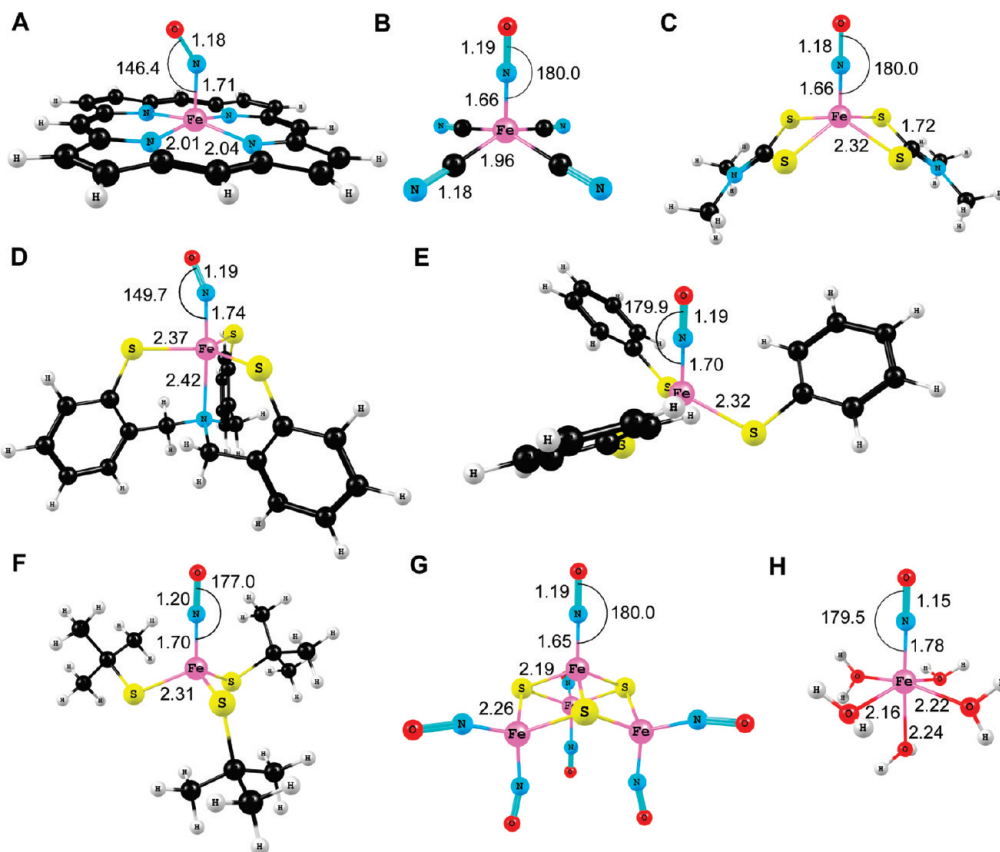


Figure 1. Molecules studied in this work and key OLYP/STO-TZP optimized geometry parameters (\AA , deg): $\text{Fe}(\text{Por})(\text{NO})$ (A, Por = porphine, $S = 1/2$, C_s), $[\text{Fe}(\text{CN})_4(\text{NO})]^{2-}$ (B, $S = 1/2$, C_{4v}), $\text{Fe}(\text{dtc-Me}_2)_2(\text{NO})$ (C, dtc-Me₂ = N,N' -dimethylidithiocarbamate, $S = 1/2$, C_{2v}), $[\text{Fe}(\text{NS3})(\text{NO})]^-$ (D, NS3 = $\text{N}(\text{CH}_2\text{C}_6\text{H}_4\text{S})_3^{3-}$, $S = 3/2$, C_1), $[\text{Fe}(\text{SPh})_3(\text{NO})]^-$ (E, $S = 3/2$, C_1), $[\text{Fe}(\text{S}'\text{Bu})_3(\text{NO})]^-$ (F, $S = 3/2$, C_1), $[\text{FeAs}_3(\text{NO})]^-$ (G, broken-symmetry $S = 0$, C_{3v}), $[\text{Fe}(\text{H}_2\text{O})_5(\text{NO})]^{2+}$ (H, $S = 3/2$, C_1). Color code for atoms: C (black), N (cyan), H (ivory), O (red), S (yellow), and Fe (magenta).

trans to the NO.²⁴ The interesting question, then, is whether the presence of the trans ligand upsets our view of metal d_{z^2} – p_z mixing as the key determinant of the observed linearity of the {FeNO}⁷ complexes mentioned above. The answer, we believe, is “not much”, but it is an interesting twist in the overall story.

Methods

In general, all calculations were carried out with a spin-unrestricted formalism, the OLYP generalized gradient approximation (GGA), Slater-type triple- ζ plus polarization (TZP) basis sets, a fine mesh for numerical integration of matrix elements, and full geometry optimizations, all as implemented in the ADF 2007²⁵ program system. For the $[\text{Fe}(\text{H}_2\text{O})_5(\text{NO})]^{2+}$ complex, geometry optimization was performed in the presence of a solvent (COSMO,²⁶ methanol, $\epsilon = 32.6$). Molecular orbitals, spin densities, and geometries were visualized with Chemcraft.²⁷

FeNO bending potentials were computed by constraining the Fe–N–O angle to fixed values (120 to 180°), while optimizing all other internal coordinates. For Roussin’s black salt, an $M_S = 0$ broken-symmetry calculation was performed at each geometry point along the bending potential curve. These calculations involved SCF optimization of the corresponding high-spin $M_S = 3$ state (where the $S = 3/2$ {FeNO}⁷ unit and the three $S = 1/2$ {Fe(NO)₂}⁹ units all have parallel spins), followed by a spin-flip to generate the antiferromagnetically coupled broken symmetry ($M_S = 0$) state.²⁸ The spin-flipped electronic structure was then used, for each fixed FeNO angle, as a starting guess for geometry optimization of the broken-symmetry state.

Figure 1 presents key optimized geometry parameters and Mulliken spin populations for the complexes studied, while Figure 3 presents the corresponding spin density plots. Key atomic spin populations are listed in Table 1.

Results

(a) **Nitrosylheme (A).** Five- and six-coordinate {FeNO}⁷ porphyrins have been intensively studied by spectroscopic and quantum chemical means.^{6–8} In this study, we have limited ourselves to an MO analysis of five-coordinate nitrosylheme.

Figure 4 depicts the bending potential of $\text{Fe}(\text{Por})(\text{NO})$, along with those of two $S = 1/2$ nonheme complexes with linear {FeNO}⁷ units. Although the calculations nicely reproduce an FeNO angle of about 145°, as observed for {FeNO}⁷ porphyrins, the minimum is shallow.⁶ Thus, moderate deviations of up to 15° or so, relative to theoretical, optimized FeNO angles, are entirely within reason for nitrosylheme crystal structures.

Figure 5, which presents the MO Walsh diagram for $\text{Fe}(\text{Por})(\text{NO})$, confirms what has been long known; as the FeNO unit is bent, the character of the HOMO changes from a σ -antibonding interaction between the Fe d_{z^2} orbital and the NO lone pair to a σ -bonding interaction between the Fe d_{z^2} orbital and the NO π^* orbital. This results in a lowering of the HOMO orbital energy by over 0.6 eV as the FeNO angle is bent from linearity down to 120°.²⁹ In contrast, the other metal d-based MOs shown in Figure 5 are destabilized, mildly to moderately, as the FeNO angle is bent as a result of weakening σ - and π -bonding interactions. The bent minimum-energy geometry

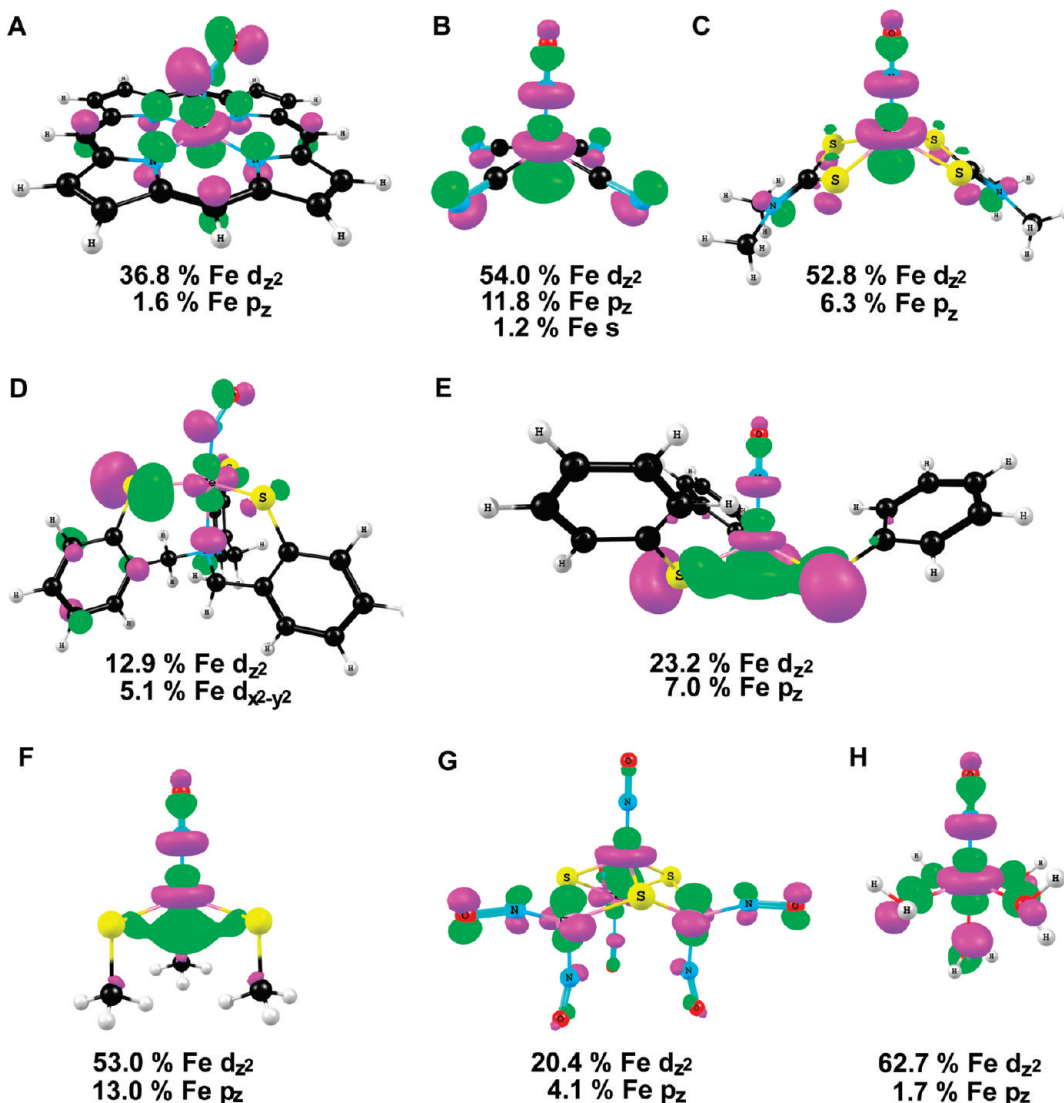


Figure 2. Highest occupied (majority spin) d_σ -based molecular orbitals for (A–H) (OLYP/STO-TZP, contour value 0.05 e \AA^3). For the purposes of this figure, the *t*Bu groups of (F) were replaced by Me, and the resulting complex was optimized with a C_{3v} symmetry constraint.

thus reflects a superposition of opposing effects, with the stabilization of the HOMO winning out by a narrow margin.

(b) $[\text{Fe}(\text{CN})_4(\text{NO})]^{2-}$ (B) and $\text{Fe}(\text{dtc-Me}_2)_2(\text{NO})$ (C).^{10,11} Figure 4 shows that DFT clearly succeeds in reproducing the approximately linear FeNO geometries of these two classic nonheme $S = 1/2 \{\text{FeNO}\}^7$ complexes. However, as in the case of nitrosylhemes, the minima are broad and shallow. For $[\text{Fe}(\text{CN})_4(\text{NO})]^{2-}$, the linearity of the $\{\text{FeNO}\}^7$ unit appears to be related to a significant amount of Fe p_z character mixing in with the predominantly Fe d_{z^2} -based HOMO. As shown in Figure 2B and C, this $d-p$ mixing results in a swollen “bottom lobe” of the d_{z^2} orbital and a shrunken “top lobe”. The latter is responsible for reduced antibonding interaction between the Fe d_{z^2} orbital and the NO lone pair, which, as we suggested, is ultimately responsible for the linearity of the $\{\text{FeNO}\}^7$ units in these two complexes.¹¹

The Walsh diagram for $\text{Fe}(\text{dtc-Me}_2)_2(\text{NO})$ is shown in Figure 6. Superficially, it looks remarkably similar to that for $\text{Fe}(\text{Por})(\text{NO})$. For both molecules, the orbital energies of the d -based MOs rise and fall in much the same manner with FeNO bending. Careful examination of the Walsh curves, however, reveals a subtle but significant difference between $\text{Fe}(\text{dtc-Me}_2)_2(\text{NO})$ and $\text{Fe}(\text{Por})(\text{NO})$. As the FeNO unit of $\text{Fe}(\text{dtc-Me}_2)_2(\text{NO})$ is bent from linearity to 120°, the orbital energy of the d_{z^2} -based HOMO is lowered by about 0.46 eV, compared to about 0.6 eV in the nitrosylheme case. The difference of 0.14 eV or 3.2 kcal/mol is not large, but it is sufficient to account for the difference in FeNO geometry in the two cases. Thus, our hypothesis that the detailed HOMO topology serves as a predictor of FeNO geometry appears to have some support in Walsh diagram analyses.³⁰

(c) Trithiolato- and Trithiolatoamine-Supported $\{\text{FeNO}\}^7$ (D–F). In a recent study, we suggested that the topology of the d_σ -based HOMO also provides a rationale for the linearity of certain $S = 3/2 \{\text{FeNO}\}^7$ units.^{9,31} Thus, DFT calculations were able to reproduce the near-linear FeNO geometry of the pseudotetrahedral $[\text{Fe}(\text{S}^{\text{t}}\text{Bu})_3(\text{NO})]^-$ complex and the bent geometry of the closely related trigonal bipyramidal $[\text{Fe}(\text{NS}^{\text{t}}\text{S})_3(\text{NO})]^-$ ($\text{NS}^{\text{t}}\text{S} = \text{N}(\text{CH}_2\text{C}_6\text{H}_4\text{S})_3^{3-}$) complex.⁹ These calculations have now been repeated with OLYP/TZP so that the results may be directly compared with other results obtained herein. Figure 7 presents the OLYP/TZP bending potentials (although the Walsh diagrams are not shown in the interest of brevity). These potentials provide an explicit measure of the flexibility of $S = 3/2 \{\text{FeNO}\}^7$ units with respect to FeNO bending, in relation to their $S = 1/2$ congeners. Judged by

$\text{Me}_2)_2(\text{NO})$ is bent from linearity to 120°, the orbital energy of the d_{z^2} -based HOMO is lowered by about 0.46 eV, compared to about 0.6 eV in the nitrosylheme case. The difference of 0.14 eV or 3.2 kcal/mol is not large, but it is sufficient to account for the difference in FeNO geometry in the two cases. Thus, our hypothesis that the detailed HOMO topology serves as a predictor of FeNO geometry appears to have some support in Walsh diagram analyses.³⁰

(c) Trithiolato- and Trithiolatoamine-Supported $\{\text{FeNO}\}^7$ (D–F). In a recent study, we suggested that the topology of the d_σ -based HOMO also provides a rationale for the linearity of certain $S = 3/2 \{\text{FeNO}\}^7$ units.^{9,31} Thus, DFT calculations were able to reproduce the near-linear FeNO geometry of the pseudotetrahedral $[\text{Fe}(\text{S}^{\text{t}}\text{Bu})_3(\text{NO})]^-$ complex and the bent geometry of the closely related trigonal bipyramidal $[\text{Fe}(\text{NS}^{\text{t}}\text{S})_3(\text{NO})]^-$ ($\text{NS}^{\text{t}}\text{S} = \text{N}(\text{CH}_2\text{C}_6\text{H}_4\text{S})_3^{3-}$) complex.⁹ These calculations have now been repeated with OLYP/TZP so that the results may be directly compared with other results obtained herein. Figure 7 presents the OLYP/TZP bending potentials (although the Walsh diagrams are not shown in the interest of brevity). These potentials provide an explicit measure of the flexibility of $S = 3/2 \{\text{FeNO}\}^7$ units with respect to FeNO bending, in relation to their $S = 1/2$ congeners. Judged by

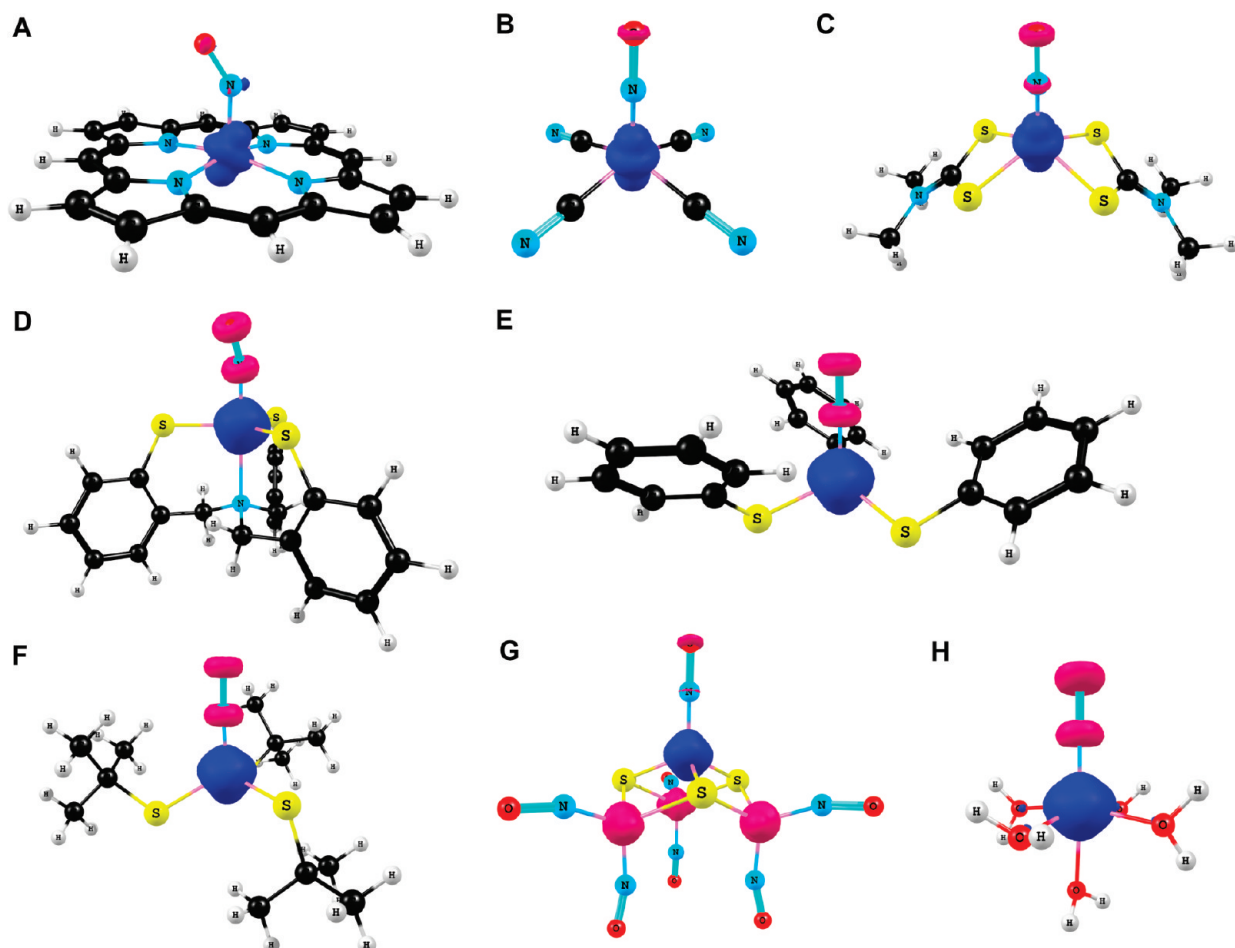


Figure 3. OLYP/STO-TZP spin density isocontours ($0.03 \text{ e}/\text{\AA}^3$); (A–H) majority and minority spin densities are indicated in blue and red, respectively.

TABLE 1: Spin Populations on $\{\text{FeNO}\}^7$ Units of Optimized Equilibrium Structures (OLYP/TZP)

complex	Fe	N	O
Fe(Por)(NO)	1.11	-0.03	-0.08
$[\text{Fe}(\text{CN})_4(\text{NO})]^{2-}$	1.25	-0.13	-0.10
$\text{Fe}(\text{dtc-Me}_2)_2(\text{NO})$	1.32	-0.17	-0.15
$[\text{Fe}(\text{N}_3)_3(\text{NO})]^-$	3.00	-0.33	-0.27
$[\text{Fe}(\text{S'Bu})_3(\text{NO})]^-$	2.97	-0.38	-0.28
$[\text{Fe}(\text{SPh})_3(\text{NO})]^-$	2.95	-0.38	-0.29
Roussin's black salt, $M_S = 0$	1.08	-0.15	-0.12
$[\text{Fe}(\text{H}_2\text{O})_5(\text{NO})]^{2+}$	3.56	-0.43	-0.39

steepness of the potential curves, the two groups of complexes are found to be comparably flexible, an interesting similarity when one considers the chemical differences between the $S = 1/2$ and $3/2$ families. It may be recalled that $S = 3/2$ complexes with linear $\{\text{FeNO}\}^7$ units are exceedingly air- and light-sensitive, in sharp contrast to their comparatively rugged $S = 1/2$ analogues.^{9,12,13} The difference in photostability, however, is an issue that falls outside the scope of the present study.

A brief comment is in order on $[\text{Fe}(\text{SPh})_3(\text{NO})]^-$ (E),¹³ which exhibits a crystallographically observed FeNO angle of 164° , which is significantly more bent than the 174° angle found for $[\text{Fe}(\text{S'Bu})_3(\text{NO})]^-$.¹² Given the flatness of the potential curves (Figure 7), the variability of the FeNO angle is not at all surprising. Nevertheless, we carefully searched the Kohn–Sham orbitals for specific orbital interactions involving the phenyl groups that could conceivably affect the FeNO angle. No such interactions, however, were found.

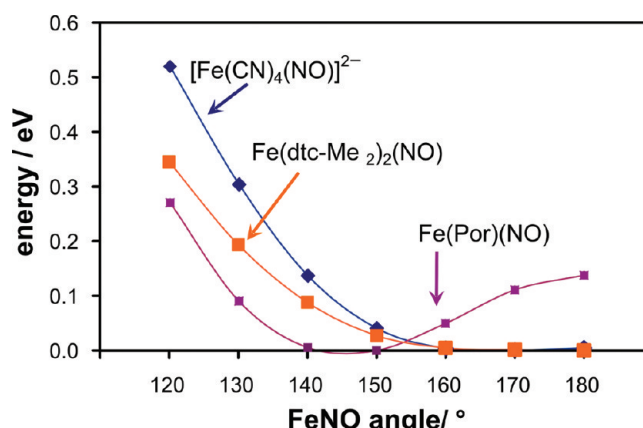


Figure 4. Potential energy curves for low-spin ($S = 1/2$) $\{\text{FeNO}\}^7$ complexes $\text{Fe}(\text{dtc-Me}_2)_2(\text{NO})$ (orange), $\text{Fe}(\text{Por})(\text{NO})$ (violet), and $[\text{Fe}(\text{CN})_4(\text{NO})]^{2-}$ (blue)) as a function of the $\text{Fe}-\text{N}-\text{O}$ angle, all other internal coordinates being optimized at each data point shown.

(d) Special Cases: Roussin's Black Salt Anion (G) and the Brown Ring Complex (H). Roussin's black salt anion, $[\text{Fe}_4(\mu-\text{S})_3(\text{NO})_7]^-$, is a diamagnetic ($S = 0$) C_{3v} species that is best described as an $S = 3/2$ $\{\text{FeNO}\}^7$ unit antiferromagnetically coupled to three $S = 1/2$ $\{\text{Fe}(\text{NO})_2\}^9$ units that are mutually ferromagnetically coupled. Broken-symmetry ($M_S = 0$) DFT works well on this electronically rather complex anion,¹⁸ and we determined the bending potential of the unique $\{\text{FeNO}\}^7$ unit using symmetry-unconstrained OLYP/TZP optimizations. The bending potential is shown in Figure 7, and the conjecture

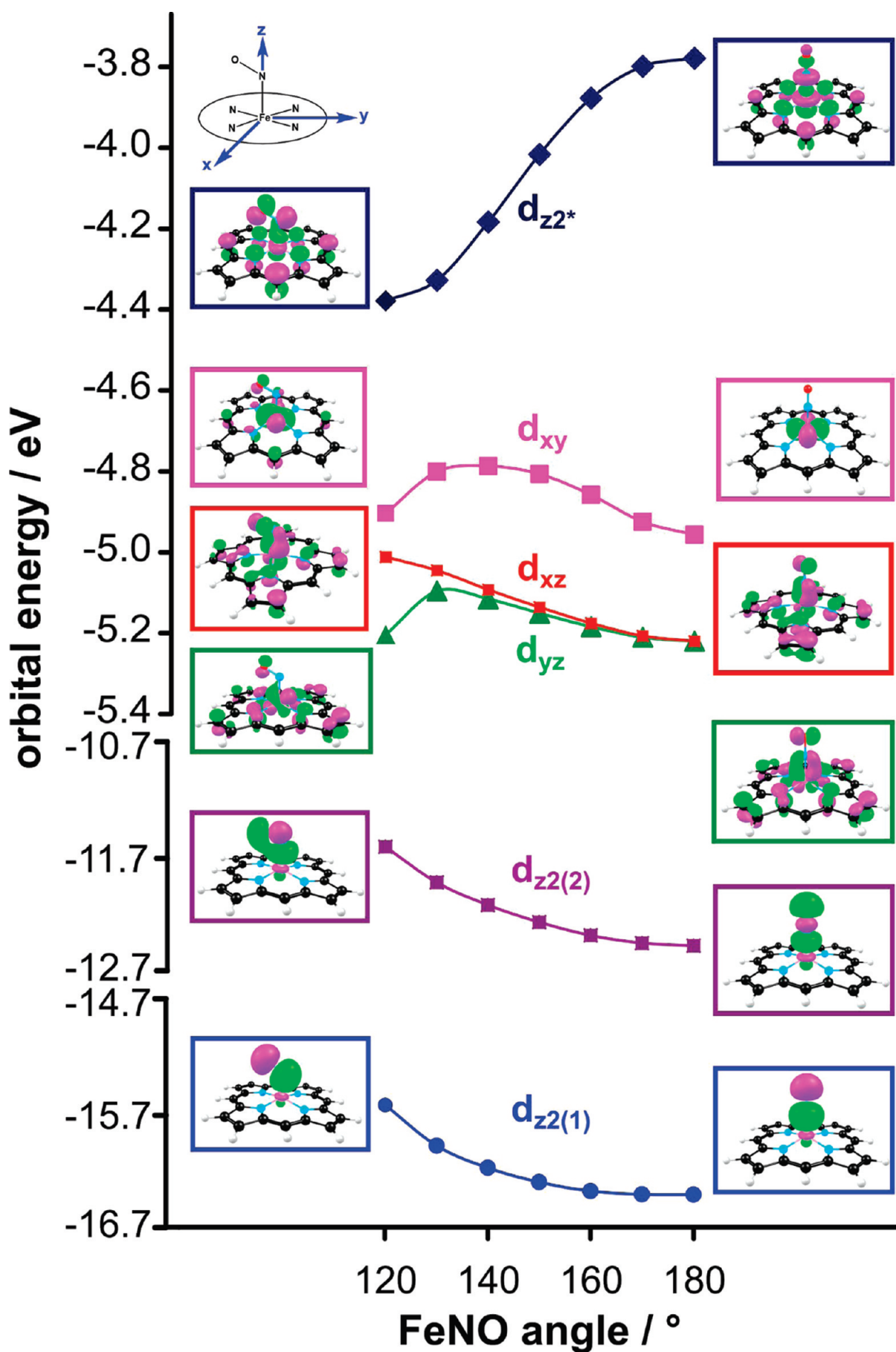


Figure 5. Walsh diagram for $[\text{Fe}(\text{Por})(\text{NO})]$. The top part of the orbital energy scale is expanded 3.5 times relative to the bottom part. All of the MOs are pictured according to the orientation depicted at the top left corner of the diagram, except for the d_{xz} -based MO (by a red border), which is rotated by 45° to provide a clearer view. The calculations underlying this diagram were carried out under C_s symmetry, and all of the MOs shown are A' , except for the d_{xz} -based MO, which is A'' .

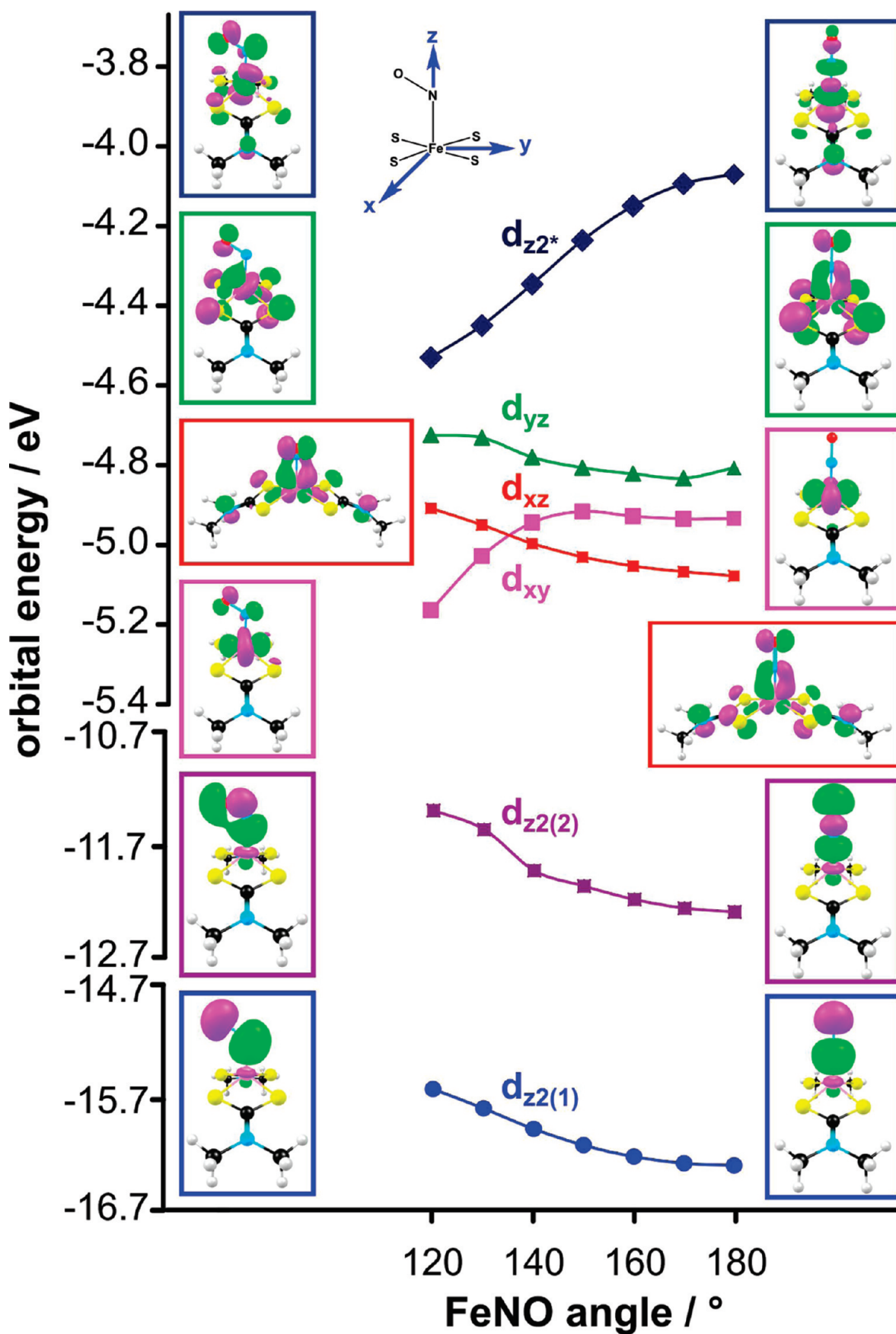


Figure 6. Walsh diagram for $\text{Fe}(\text{dtc-Me}_2)_2(\text{NO})$. The top part of the orbital energy scale is expanded 3.5 times relative to the bottom part. All of the MOs are pictured according to the orientation indicated at the top of the diagram, except for the d_{xz} -based MO (by a red border), which is rotated by 90° to provide a clearer view. The calculations underlying this diagram were carried out under C_s symmetry, and all of the MOs shown are A' except for the d_{xz} -based MO, which is A'' .

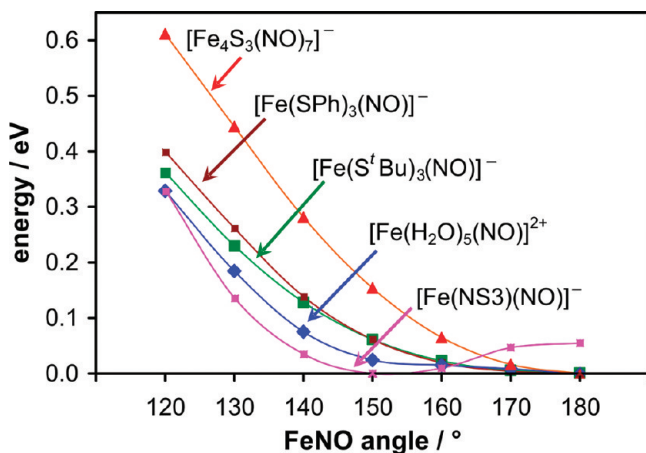


Figure 7. Potential energy curves for high-spin ($S = 3/2$) $\{\text{FeNO}\}^7$ complexes ($[\text{Fe}(\text{NS3})(\text{NO})]^-$ (magenta), $[\text{Fe}(\text{H}_2\text{O})_5(\text{NO})]^{2+}$ (blue), $[\text{Fe}(\text{SBu})_3(\text{NO})]^-$ (green), $[\text{Fe}(\text{SPh})_3(\text{NO})]^-$ (brown), and $[\text{Fe}_4\text{S}_3(\text{NO})]^-$ (red)) as a function of the Fe–N–O angle, all other internal coordinates being optimized at each data point shown.

that this anion might behave unusually appears to be borne out. Thus, the bending potential is much steeper than that for the other $\{\text{FeNO}\}^7$ complexes studied, be they $S = 1/2$ or $3/2$. Figure 8 presents broken-symmetry spin density plots, key geometry parameters, and Mulliken spin populations for the C_{3v} and a highly bent conformation of the Roussin black salt anion ($\angle \text{FeNO} = 120^\circ$). As the FeNO angle is bent, it is clear that the absolute values of the spin populations increase dramatically, showing that the α and β spins are increasingly decoupled. Thus, the linear geometry is favored not only on stereochemical grounds but also because such a geometry corresponds to maximum spin coupling between the iron centers.

The brown ring complex is unusual in that DFT calculations indicate an essentially linear $\{\text{FeNO}\}^7$ unit, despite the presence of a trans water ligand.²³ An examination of the Kohn–Sham MOs showed that the Fe d_{z^2} -based HOMO does not, in fact, have significant Fe p_z character. Again, to understand the linearity of the $\{\text{FeNO}\}^7$ unit, we resorted to a Walsh diagram

analysis (details not shown), which showed that the MO orbital energies behave in much the same way as those for the complexes discussed above that do not have trans ligands. Thus, a linear $S = 3/2$ $\{\text{FeNO}\}^7$ unit may in fact be compatible with the presence of a very weak trans ligand such as water. As soon as the trans ligand becomes somewhat stronger as in the NS3 complex, a bent minimum is favored. Of course, the potential energy minima are exceedingly flat for both the brown ring complex and the NS3 complex; in fact, they are the flattest potentials found in this study, almost certainly reflecting the remarkably subtle balance of opposing effects in the Walsh diagrams in question.

Concluding Remarks

We have provided here a unified MO exploration of relatively unusual $\{\text{FeNO}\}^7$ complexes, both $S = 1/2$ and $3/2$, that exhibit linear or quasi-linear FeNO units. In essence, we have attempted to answer the question whether the bonding in such complexes is special in any way, relative to that in their bent counterparts. MO analyses indicate that the bonding is indeed somewhat special in these complexes. The great majority of these complexes do not have a ligand trans to the NO. This results in an infusion of metal p_z character into the d_{z^2} -based HOMO, which reduces its antibonding interaction with the NO lone pair. This appears to be the single most common factor responsible for the linearity of the FeNO groups in the complexes in question.

It is worth noting again that DFT does an excellent job of capturing the structural chemistry of iron nitrosyls.^{5,8–11,29} This is all the more remarkable when one considers the general flatness of the bending potentials at the bottom of the potential wells. The observed geometries, whether linear or bent, reflect a superposition of multiple MO energies that rise or fall as the FeNO unit bends away from linearity. Walsh diagram analyses indicate that these opposing effects are delicately balanced, resulting in unusually flat FeNO bending potentials. Under the circumstances, it is gratifying that the HOMO topology and orbital energy serve as a simple indicator of whether the FeNO unit should be linear or bent.³⁰

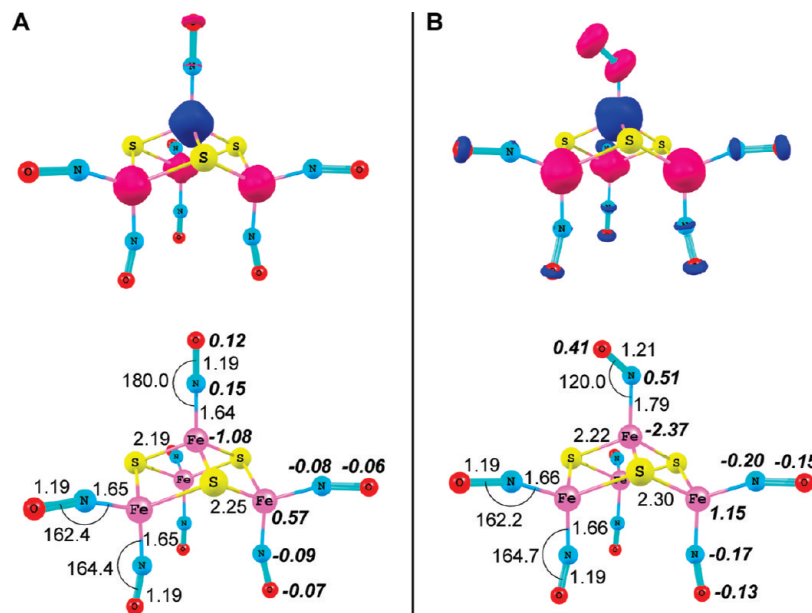


Figure 8. Selected results on Roussin's black salt anion, $[\text{Fe}_4\text{S}_3(\text{NO})]^-$ (OLYP/TZP, $M_S = 0$, C_1). Spin density of the (A) equilibrium geometry (C_{3v}) and (B) constrained geometry Fe–N–O angle 120° (C_1). Bond distances (\AA) and angles (deg) are shown with a normal font, whereas Mulliken spin populations are shown in bold italic for the equilibrium geometry (C_{3v}) and constrained geometry (C_1) with an Fe–N–O angle of 120° .

Acknowledgment. This work was supported by the Research Council of Norway (A.G., K.H.H.) and the National Research Fund of the Republic of South Africa (J.C., Grant No. 65507). We thank Professor John Enemark of The University of Arizona for his comments on an early version of this article.

Supporting Information Available: Optimized Cartesian coordinates for selected systems. This material is available free of charge via the Internet at <http://pubs.acs.org>.

References and Notes

- (1) The number 7 refers to the so-called Enemark–Feltham electron count, which is the sum of the numbers of the metal d and NO π^* electrons; see Westcott, B. L.; Enemark, J. H. In *Inorganic Electronic Structure and Spectroscopy*; Solomon, E. I., Lever, A. B. P., Eds.; Wiley: New York, 1999; Vol. 2, pp 403–450, and references therein.
- (2) For a survey of metalloporphyrin-NO_x structures, see: Wyllie, G. R. A.; Scheidt, W. R. *Chem. Rev.* **2002**, *102*, 1067–1090.
- (3) NO biology: (a) *Nitric Oxide: Biology and Pathobiology*; Ignarro, L., Ed.; Academic: San Diego, CA, 2000; pp 3–19. (b) Butler, A.; Nicholson, R. *Life, Death and Nitric Oxide*; The Royal Society of Chemistry: Cambridge, U.K., 2003. (c) *The Smallest Biomolecules: Diatomics and Their Interactions with Heme Proteins*; Ghosh, A., Ed.; Elsevier: Amsterdam, The Netherlands, 2008; pp 1–603.
- (4) McCleverty, J. A. *Chem. Rev.* **2004**, *104*, 403–418.
- (5) Reviews on DFT calculations on nitrosyls: (a) Ghosh, A.; Hopmann, K. H.; Conradie, J. In *Computational Inorganic and Bioinorganic Chemistry*; Solomon, E. I., Scott, R. A., King, R. B., Eds.; John Wiley & Sons, Ltd: Chichester, U.K., 2009; pp 389–410. (b) Ghosh, A. *Acc. Chem. Res.* **2005**, *38*, 943–954.
- (6) (a) Ellison, M. K.; Scheidt, W. R. *J. Am. Chem. Soc.* **1997**, *119*, 7404–7405. (b) Scheidt, W. R.; Ellison, M. K. *Acc. Chem. Res.* **1999**, *32*, 350–359. (c) Hayes, R. G.; Ellison, M. K.; Scheidt, W. R. *Inorg. Chem.* **2000**, *39*, 3665–3668.
- (7) Ghosh, A.; Wondimagegn, T. *J. Am. Chem. Soc.* **2000**, *122*, 8101–8102.
- (8) (a) Paulat, F.; Lehnert, N. *Inorg. Chem.* **2007**, *46*, 1547–1549. (b) Praneeth, V. K. K.; Näther, C.; Peters, G.; Lehnert, N. *Inorg. Chem.* **2006**, *45*, 2795–2811.
- (9) Conradie, J.; Quarless, D. A., Jr.; Hsu, H.-F.; Harrop, T. C.; Lippard, S. J.; Koch, S. A.; Ghosh, A. *J. Am. Chem. Soc.* **2007**, *129*, 10446–10456.
- (10) Butcher, R. J.; Sinn, E. *Inorg. Chem.* **1980**, *19*, 3622–3626.
- (11) Conradie, J.; Ghosh, A. *J. Inorg. Biochem.* **2006**, *100*, 2069–2073.
- (12) Harrop, T. C.; Song, D.; Lippard, S. J. *J. Am. Chem. Soc.* **2006**, *128*, 3528–3529.
- (13) Lu, T.-T.; Chiou, S.-J.; Chen, C.-Y.; Liaw, W.-F. *Inorg. Chem.* **2006**, *45*, 8799–8806.
- (14) Klein, D. P.; Young, V. G., Jr.; Tolman, W. B.; Que, L., Jr. *Inorg. Chem.* **2006**, *45*, 8006–8008.
- (15) D'Addario, S.; Demartin, F.; Grossi, L.; Iapalucci, M. C.; Laschi, F.; Longoni, G.; Zanello, P. *Inorg. Chem.* **1993**, *32*, 1153–1160.
- (16) (a) Sanina, N. A.; Chuev, I. I.; Aldoshin, S. M.; Ovanasyan, N. S.; Strelets, V. V.; Geleti, Yu. V. *Russ. Chem. Bull.* **2000**, *49*, 444–451. (b) Sanina, N. A.; Aldoshin, S. M. *Russ. Chem. Bull. Int. Ed.* **2004**, *53*, 2428–2448.
- (17) Jaworska, M.; Stasicka, Z. *J. Mol. Struct.* **2006**, *785*, 68–75.
- (18) Hopmann, K. H.; Conradie, J.; Ghosh, A. *J. Phys. Chem. B* **2009**, *113*, 10540–10547.
- (19) Hopmann, K. H.; Noddleman, L. H.; Ghosh, A. *Chem.—Eur. J.* **2010**, In press.
- (20) The OPTX exchange functional: Handy, N. C.; Cohen, A. *J. Mol. Phys.* **2001**, *99*, 403–412.
- (21) The LYP correlation functional: Lee, C.; Yang, W.; Parr, R. G. *Phys. Rev. B* **1988**, *37*, 785–789.
- (22) By comparison, carbonyl tilting and bending has been much more thoroughly studied by computational means: (a) Ghosh, A.; Bocian, D. F. *J. Phys. Chem.* **1996**, *100*, 6363–6367. (b) Spiro, T. G.; Kozlowski, P. M. *Acc. Chem. Res.* **2001**, *34*, 137–144.
- (23) One instructive example that we will not discuss at length in this study is $S = 1/2 \{FeNO\}^7$ 5,5-tropocoronand, where the linearity of the FeNO group was ascribed to half-occupancy of a stereochemically less active Fe $d_{z^2-z^2}$ orbital as opposed to a d_{z^2} orbital (the z direction being identified with the FeNO axis): (a) Franz, K. J.; Lippard, S. J. *J. Am. Chem. Soc.* **1999**, *121*, 10504–10512. (b) Franz, K. J.; Lippard, S. J. *J. Am. Chem. Soc.* **2001**, *123*, 1266. (c) Tangen, E.; Conradie, J.; Ghosh, A. *Inorg. Chem.* **2005**, *44*, 8699–8706.
- (24) (a) Wanat, A.; Schneppensieper, T.; Stochel, G.; van Eldik, R.; Bill, E.; Wieghardt, K. *Inorg. Chem.* **2002**, *41*, 4–10. (b) Cheng, H.-Y.; Chang, S.; Tsai, P.-Y. *J. Phys. Chem. A* **2004**, *108*, 358–361.
- (25) Velde, G. T.; Bickelhaupt, F. M.; Baerends, E. J.; Guerra, C. F.; Van Gisbergen, S. J. A.; Snijders, J. G.; Ziegler, T. J. *Comput. Chem.* **2001**, *22*, 2001.
- (26) (a) Klamt, A.; Schüürmann, G. *J. Chem. Soc.: Perkin Trans.* **1993**, *2*, 799–805. (b) Klamt, A. *J. Phys. Chem.* **1995**, *99*, 2224–2235. (c) Klamt, A.; Jones, V. *J. Chem. Phys.* **1996**, *105*, 9972–9981.
- (27) ChemCraft: <http://www.chemcraftprog.com>.
- (28) Schmitt, E. A.; Noddleman, L.; Baerends, E. J.; Hendrickson, D. N. *J. Am. Chem. Soc.* **1992**, *114*, 6109–6119.
- (29) Unlike the d_{z^2} -based HOMO, two other d_{z^2} -based bonding MOs, denoted $d_{z^2(1)}$ and $d_{z^2(2)}$ in Figures 5 and 6, are destabilized by FeNO bonding.
- (30) As to the wisdom of attempting to explain such a subtle domain of results, we cannot do better than quote Hoffmann's advice: Hoffmann, R. *J. Mol. Struct.: THEOCHEM* **1998**, *428*, 1–6. “I can only give you the advice: try, please try. Take the existential plunge, the hazard of proving an explanation. Do numerical experiments to probe your wild notion, to be sure, but don't be afraid, forward a simple explanation.”
- (31) For key experimental and computational studies of nonheme $\{FeNO\}^7$ units, see, for example: (a) Brown, C. A.; Pavlovsky, M. A.; Westre, T. E.; Zhang, Y.; Hedman, B.; Hodgson, K. O.; Solomon, E. I. *J. Am. Chem. Soc.* **1995**, *117*, 715–732. (b) Li, M.; Bonnet, D.; Bill, E.; Neese, F.; Weyhermüller, T.; Blum, N.; Sellmann, D.; Wieghardt, K. *Inorg. Chem.* **2002**, *41*, 3444–3456. (c) Garcia Serres, R.; Grapperhaus, C. A.; Bothe, E.; Bill, E.; Weyhermüller, T.; Neese, F.; Wieghardt, K. *J. Am. Chem. Soc.* **2004**, *126*, 5138–5153.

JP101847Y